Journal of Applied Electrochemistry (2019) 49:195–205
https://doi.org/10.1007/s10800-018-1259-2

RESEARCH ARTICLE

Electrochemical detection of Cr(VI) with carbon nanotubes decorated with gold nanoparticles

Carmel B. Breslin[1] · **David Branagan**[1] · **Lynn M. Garry**[1]

Received: 13 June 2018 / Accepted: 7 October 2018 / Published online: 16 October 2018

Abstract

A nanocomposite consisting of gold nanoparticles deposited on the side walls of functionalised multi-walled carbon nanotubes, *Ox*-MWCNT-Au_{nano}, was prepared using a simple chemical reduction. The nanoparticles were well dispersed with a mean diameter of 7.5 nm and had a face-centred cubic structure and a gold loading between 2.0% and 2.6% by weight. These gold decorated nanotubes were cast onto a gold electrode to form a uniform and homogeneous sensor. Using cyclic voltammetry, the reduction of Cr(VI) was observed at a peak potential of 0.52 V versus SCE in an acidified H_2SO_4 solution, pH 2.0. A linear calibration curve with a sensitivity of 0.28 mA mM^{-1} and a LOD of 7.2×10^{-7} M was obtained using constant potential amperometry coupled with rotating disc voltammetry. The electrochemical detection of Cr(VI) was also observed at a MWCNT-modified gold substrate but with a higher LOD, illustrating the advantage of combining the gold nanoparticles with MWCNTs. The sensor showed good selectivity for the detection of Cr(VI) in the presence of Cu(II), chloride and nitrates and in a real water sample. This was attributed to the electropositive reduction potentials of Cr(VI), the acidic H_2SO_4 supporting electrolyte that provides a well-known cleaning effect at gold, and the size and good dispersion of the gold nanoparticles that minimise particle agglomeration.

Graphical abstract

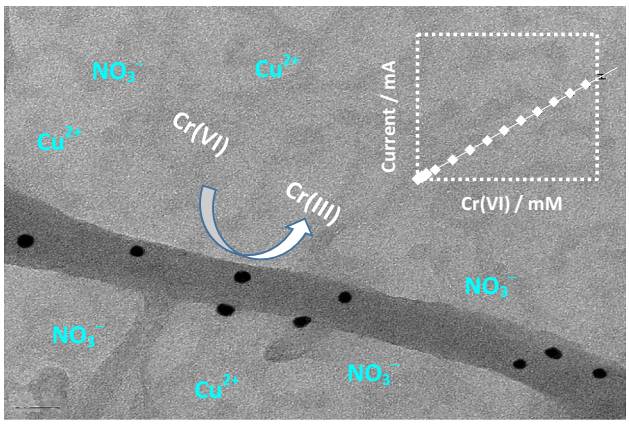

Keywords Amperometry · Carbon nanotubes · Chromium(VI) · Gold nanoparticles · Nanocomposite

1 Introduction

It is well known that Cr(VI), or hexavalent chromium, is highly toxic and it has been linked to several forms of cancer in animals and humans [1]. Due to the fact that it is a

✉ Carmel B. Breslin
Carmel.Breslin@mu.ie

[1] Department of Chemistry, Maynooth University, Maynooth, County Kildare, Ireland

strong oxidising agent, it has the potential to oxidise several analytes or biological species that it comes in contact with, making it a significant environmental pollutant [2, 3]. The World Health Organisation (WHO) has set the limit of hexavalent chromium in ground water at 50 μg L^{-1} [4]. Cr(VI) is released into the environment in acid effluents from industries involved with metal plating and leather tanning [5, 6]. Although Cr(III) is not regarded as toxic, it can be oxidised into Cr(VI) during the chlorination of water [7], adding to the concentration of Cr(VI) in water supplies and ground water. The quantification of Cr(VI) in the laboratory is generally achieved using analytical techniques such as atomic absorption spectroscopy and mass spectrometry [8, 9]. To distinguish between the Cr(III) and Cr(IV), many of these techniques rely on the formation of Cr(VI) complexes with the complexing agents 1,5-diphenylcarbazide and pyrrolidine dithiocarbamate prior to analysis [10, 11]. However, these methods are costly and not suitable for field analysis. More recent approaches include the development of optical sensors. For example, aluminosilica monoliths have been modified with diphenylcarbazide to give an immobilised receptor that is capable of capturing Cr(VI) to give highly selective and sensitive sensors [12]. Colloidal suspensions of silole nanoparticles have also been employed as selective Cr(VI) chemosensors [13]. There is also considerable interest in the development of electrochemical sensors for the quantification of Cr(VI) [14–22]. This is largely due to the fact that electrochemical sensors and indeed many of the optical sensors can be employed as portable devices, eliminating the need for large instrument analysis. While significant progress has been made in the development of optical sensors, challenges still remain, including relatively high costs and long real-time quantitative analyses. Equally, electrochemical sensors suffer from electrode instability and selectivity issues. Therefore, there is still an increasing need for the development of a portable technology that is suitable for field analyses in the sensitive and selective detection of Cr(VI).

Several modified electrodes have been employed in the electrochemical detection of Cr(VI), including poly-L-histidine modified screen-printed carbon electrodes [14], supercoiled DNA-modified mercury electrodes [15], and bismuth-plated glassy carbon electrodes [16]. The reduction of Cr(VI) and its electrochemical behaviour depends on the solution composition and the nature and composition of the electrode materials. The highly corrosive nature of Cr(VI) leads to the passivation of many electrodes. However, carbon and gold-based electrodes are generally considered as the best electrocatalysts for the Cr(VI) reduction reaction [17–19]. Welch et al. [17] compared the performance of glassy carbon, boron-doped diamond and gold electrodes for the detection of Cr(VI) and concluded that gold electrodes provided the best performance. Further reports by Tukur et al. [18], Jin et al. [19] and Jena and Raj [20] showed promising results with electrodes modified with gold nanoparticles. While there is good electrocatalytic activity for Cr(VI) reduction at gold electrodes, more promising results have been achieved with gold nanoparticles [18–20]. In terms of carbon-based electrodes, there is also interest in using carbon nanotubes in the development of Cr(VI) sensors [21]. This is largely due to their impressive range of properties, which include very high surface areas, very good conductivity and it is relatively easy to modify their surfaces. Rudnitskaya et al. [22] fabricated a lignin-poly(propylene oxide) copolymer doped with carbon nanotubes to give a Cr(VI) potentiometric sensor with a relatively low detection limit of 5.0×10^{-6} M. Both carbon nanotubes and gold nanoparticles exhibit interesting properties and their combination to form composites has gained considerable interest in recent years [23–26]. Composites fabricated through the immobilisation of gold nanoparticles on carbon nanotubes have been used to develop a number of biomedical sensors and environmental sensors for the quantification of toxic metal ions, organic and inorganic pollutants [23–26].

In this study, a composite fabricated by decorating multi-walled carbon nanotubes with crystalline gold nanoparticles, with diameters lower than 10 nm, is used in the detection of Cr(VI). This composite was chosen as both gold- and carbon-based materials have been identified previously as suitable substrates for the electrochemical reduction of Cr(VI). Furthermore, the carbon nanotubes provide a high conductivity and a high surface area that facilitates the nucleation of gold nanoparticles. No other ligands are added to give a reasonably simple modified electrode. This composite gives a limit of detection that satisfies WHO regulations and it provides good selectivity in the presence of various interferences and performs well in real water samples.

2 Experimental

Multi-walled carbon nanotubes (MWCNTs > 99% purity) and all other reagents were purchased from Sigma Aldrich. The pristine MWCNTs were purified and modified with carboxylated groups to increase their dispersion in solution by refluxing in concentrated HNO_3 at 120 °C for 24 h. The sample was then purified using centrifugation with repeated cycles of dilution with ultra-pure water, until the pH was approximately neutral. Gold nanoparticles were deposited at both the functionalised, *Ox*.MWCNTs, and the pristine carbon nanotubes, MWCNTs. These were dispersed into a 1% sodium dodecyl sulphate (SDS) solution at a concentration of 0.5 mg mL^{-1}, using ultra-sonication to yield a homogeneous and stable dispersion. The gold nanoparticles were formed by adding, with stirring, a 1% w/v $HAuCl_4 \cdot 3H_2O$ solution and then slowly adding

a 0.75% w/v $NaBH_4$ solution. After 5 min, the resulting composite material was isolated on a 0.45-µm pore size Whatman® membrane. The final materials, *Ox*.MWCNT-Au_{nano} and MWCNT-Au_{nano}, were fully dried using an infrared lamp and stored in a dry environment.

The composites were characterised using a FEI Titan TEM and a Hitachi S-3200-N SEM, energy dispersive X-Ray analysis (EDX) with an Oxford Instrument INCAx-act EDX system. For the TEM measurements, the composite was dispersed in ethanol and 20 µL of this mixture was left to dry on a carbon support on a copper grid. X-Ray diffraction (XRD) was conducted on a PANalytical X'Pert PRO MPD system. A Perkin Elmer Precisely Analyst system was used for atomic absorption spectroscopy (AA). Cyclic voltammetry was carried out on a Solartron SI 1287 potentiostat and constant potential amperometry (CPA) and rotating disc voltammetry (RDV) experiments were performed with a CH Instruments, CHI 760C potentiostat. A conventional three-electrode cell, consisting of a high surface area platinum counter electrode, a saturated calomel reference electrode, SCE, together with the modified gold electrodes, was used. Ultra-pure water obtained through a Millipore filtration system was used in all experiments.

A quantification of the surface acid groups introduced during refluxing in HNO_3 was obtained using an acid base titration. In a typical setup, the *Ox*.MWCNTs composites were dispersed in a standardised 0.01 M NaOH solution in 0.1 M NaCl, with the aid of a short sonication, and left to stir for 14 h under N_2 bubbling to displace adsorbed CO_2 from the *Ox*.MWCNTs. The reaction mixture was then filtered through a 0.45-µm pore size Whatman® syringe tip to remove the nanotubes and the remaining NaOH solution was titrated with standardised 0.01 M HCl in 0.1 M NaCl. For comparison, the titration was repeated with pristine MWCNTs. The amount of gold in the composites was measured using AA. The gold was extracted using *aqua regia* to yield a yellow coloured $HAuCl_4$-containing solution, which was then isolated in 0.1 M HCl. Standard solutions were prepared from a commercial 1000 ppm standard stock solution, which consisted of 1.00 mg of pure gold in 15% HCl.

The Cr(VI) sensors were fabricated by casting *Ox*.MWCNT-Au_{nano}, MWCNT-Au_{nano} or MWNCTs onto gold (4 mm) electrodes. A dispersion of the nanotubes (10 mg mL^{-1}) in dimethylformamide (DMF) was achieved using ultra-sonication. A volume (20 µL) of this dispersion was cast onto the electrodes and left to dry fully under an infrared lamp. The Cr(VI) solutions were prepared in H_2SO_4 and unless otherwise stated, the pH was maintained at 2.0. All experiments were repeated at least three times (n = 3) and the errors in the measurements are represented by error bars. The Cr(VI) was detected using cyclic voltammetry and CPA combined with RDV. The peak currents obtained from the cyclic voltammograms were recorded after 15 cycles to give steady-state peak currents.

3 Results and discussion

Prior to the detection of Cr(VI), the *Ox*.MWCNT-Au_{nano} and MWCNT-Au_{nano} composites were characterised to obtain information on the percentage of surface acid groups introduced during the acid functionalisation, the size, distribution and crystallinity of the gold nanoparticles and the amount of gold deposited at the carbon nanotubes.

3.1 Characterisation of composites

A typical acid-base titration curve is shown in Fig. 1, where the titration curves obtained using pristine MWCNTs and *Ox*.MWCNTs are compared. Two equivalence points (EP) are clearly visible during the titration of the *Ox*.MWCNTs. In contrast, titrations with the pristine MWCNTs yielded no indication of any measurable surface acidic functionalities. The first EP appears at approximately a pH of 8.0. This arises from the titration between the unreacted NaOH and HCl and is related to the total surface acidity of the *Ox*.MWCNTs, including that of surface adsorbed polycyclic carbonaceous fragments. These fragments become deadsorbed from the surface and appear in the NaOH filtrate as polycyclic aromatic carboxylic salts [27, 28]. Accordingly, a second EP is observed at a pH of 5.0, which can be ascribed to the protonation of these carboxylates. Using these data, the percentage of acidic group coverage was calculated as 6%. The presence of carboxylic groups on the *Ox*.MWCNTs was further confirmed by FTIR, as shown in the inset in Fig. 1, with a peak at 1725 cm^{-1} which can be assigned to the > C=O stretching mode of the carboxylic groups. Again, this is only evident with the acid functionalised *Ox*.MWCNTs.

Representative TEM micrographs are shown for the *Ox*.MWCNT-Au_{nano} at different magnifications in Fig. 2, while a distribution of the gold particles with different diameters is shown in the accompanying distribution plot. This statistical analysis was conducted on 100 random gold particles using IMAGE J software. It is evident from Fig. 2a that material aggregation occurs, but this is largely due to solvent evaporation. The gold particles appear to be reasonably well dispersed along the carbon nanotubes and there is no evidence to suggest that multiple particles nucleate at the same site, Fig. 2b, c. The size distribution histogram, Fig. 2d, shows the distribution in size ranging from 5.5 to 12.5 nm in diameter, with a mean diameter of 7.5 nm. The carbon nanotubes ranged from 15 to 20 nm in diameter and contained a degree of surface roughness which is consistent with the acid oxidation process.

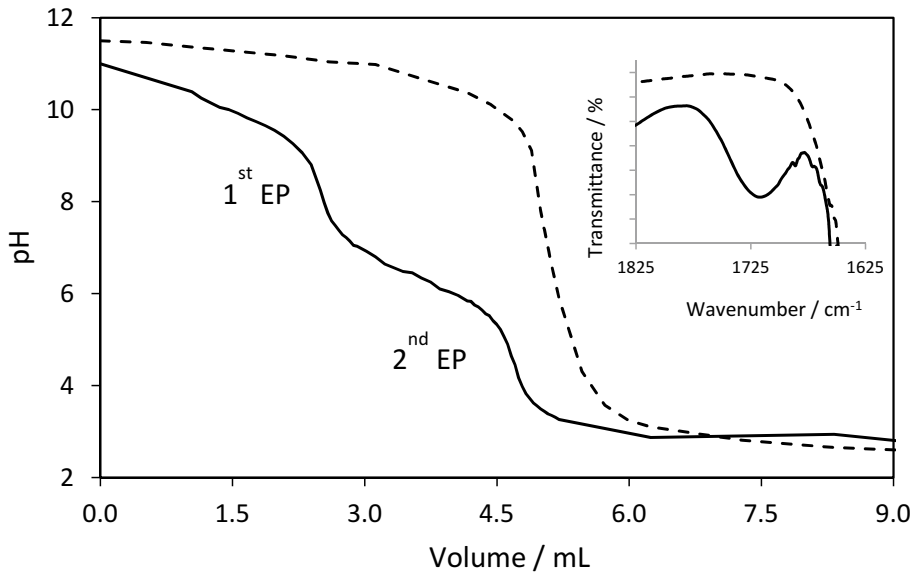

Fig. 1 Potentiometric titrations and FTIR spectra (inset) of dashed line—pristine and continuous line—*Ox*.MWCNTs

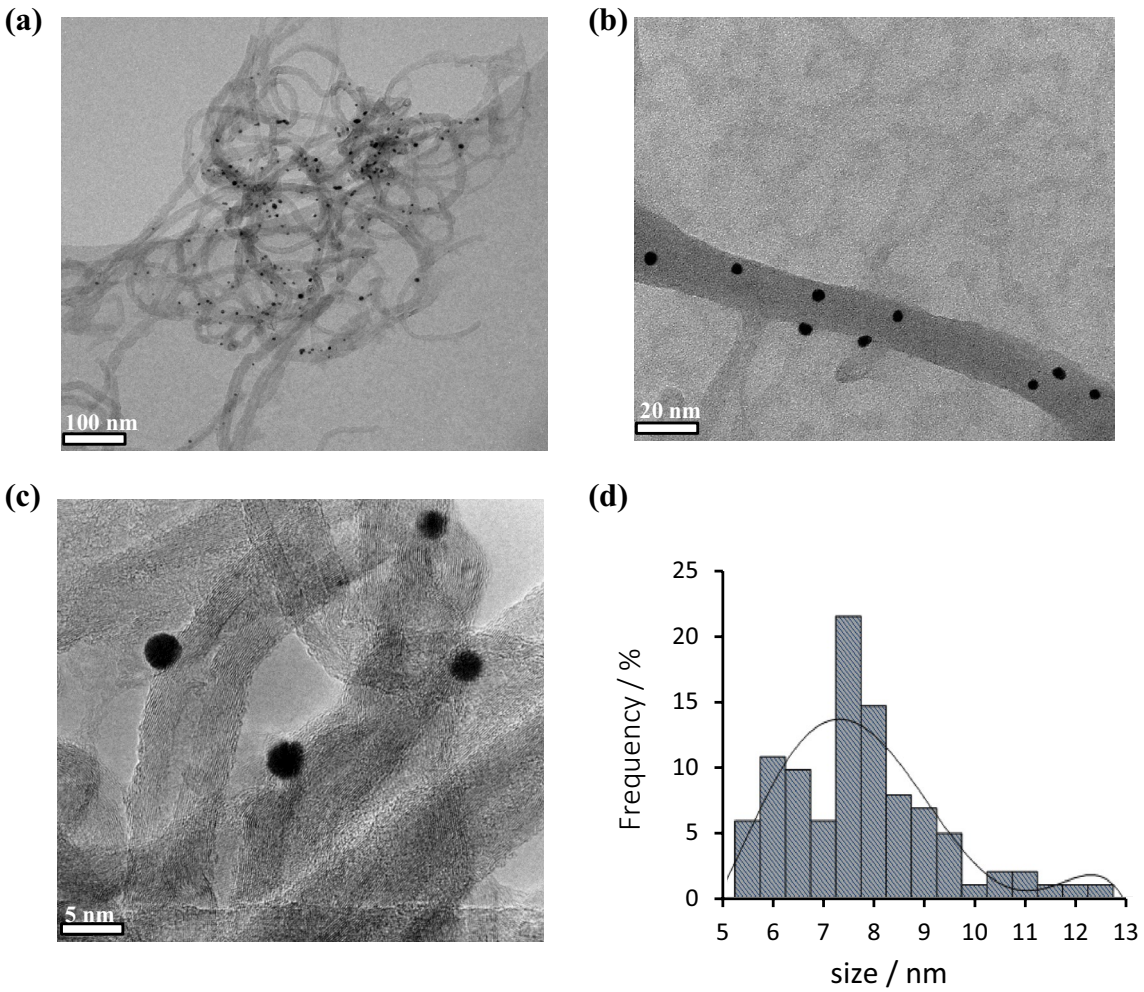

Fig. 2 TEM micrographs of the *Ox*.MWCNT-Au_{nano} composite at **a** low, **b, c** high magnifications and **d** a size-distribution histogram of the gold nanoparticles formed

An XRD spectrum of the *Ox*.MWCNT-Au_{nano} is presented in Fig. 3, where the crystalline planes are evident and these are assigned and shown on the figure. The characteristic crystalline planes of gold are apparent together with the planes corresponding to the carbon nanotubes. In particular, the reflection at 2θ = 25.84° corresponds to the (002) graphitic plane of the carbon nanotubes while those appearing at 2θ = 38.23°, 44.50°, 64.64°, 77.52° and 81.60° correspond to the (111), (200), (220), (311) and (222) planes, respectively, of the crystalline gold particles [29, 30]. It is clear that the (111) plane is the most abundant and these data indicate that the gold particles are formed predominantly with a face-centred cubic structure. The size of the gold particles was estimated using the Scherrer equation, Eq. (1), where D represents the average diameter of a spherical particle; β is the full width at half maximum of the most intense reflection, expressed in radians; θ is the position of the reflection; λ is the wavelength and 0.89 is the Scherrer constant [31]. The most intense reflection at 38.23°, corresponding to the (111) plane of gold, was used to calculate θ, and the value of β was also measured using this signal. A value of 1.541874 Å was used for the X-Ray wavelength, λ. Using this analysis, it was found that the gold particles had an approximate particle size of 7.92 nm, which agrees well with the TEM results showing the largest frequency distribution occurring at 7.50 nm.

$$D = \frac{0.89\lambda}{\beta\cos\theta} \quad (1)$$

Using atomic absorption spectroscopy, AA and SEM-EDX, the gold loadings in the *Ox*.MWCNT-Au_{nano} and MWCNT-Au_{nano} were estimated. Although EDX is not a quantitative technique, it was used in combination with the AA data, to give a loading estimate. In the EDX spectrum (not shown) the characteristic peak at 2.2 keV was observed for the gold particles. Using the EDX data, a gold loading of 2.6% was obtained, while a slightly lower loading of 2.0% was calculated using the AA data for *Ox*.MWCNT-Au_{nano}. A lower loading of 1.0% was estimated for the MWCNT-Au_{nano} composite using AA analysis. The lower loading with the pristine carbon nanotubes is consistent with the poor dispersion of these nanotubes in solution.

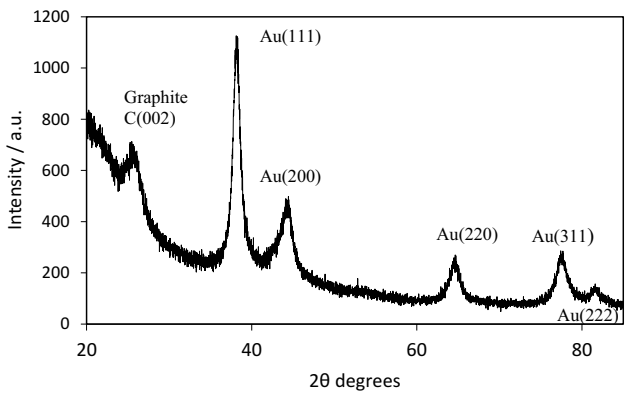

Fig. 3 XRD spectrum of the *Ox*.MWCNT-Au_{nano} composite

3.2 Formation of the Cr(VI) sensor

The modified electrodes for the detection of Cr(VI) were prepared by dispersing the gold decorated nanotubes in DMF using 10 mg mL^{-1} and ultra-sonication for 30 min. A 20 µL of this dispersion was cast onto the electrode surface and dried fully under an infrared lamp. SEM micrographs of this cast deposit at two different magnifications are shown in Fig. 4. As evident from the micrographs, the cast composites appear uniform with no evidence of significant structural inhomogeneities. In the higher magnification micrograph, Fig. 4b, individual carbon nanotubes are visible and they appear to be aligned randomly on the surface.

The mapping profiles for C and Au are shown in the inset of Fig. 4a, where the light coloured segments indicate the presence of the element. For these analyses, the gold-decorated nanotubes were dispersed on a platinum electrode to eliminate interference from the gold substrate. As expected, the C is well dispersed across the surface and in high concentrations. Less gold is detected and while there are areas with somewhat lower concentrations of gold, it is generally well dispersed across the surface. The percentages of C, Au and O, obtained for the pristine MWCNT, gold decorated MWCNT and the gold decorated functionalised MWCNT-modified electrodes are presented in Table 1. It is clear from this table that the O content increases on oxidation and functionalisation of the nanotubes, *Ox*.MWCNT-Au_{nano}, which is associated with the introduction of the carbonyl groups. The Au content of *Ox*.MWCNT-Au_{nano} at 2.86% is in very good agreement with the analysis of the synthesised composite, indicating that no gold is lost on formation of the modified electrodes. It is also clear that more gold is deposited at the functionalised carbon nanotubes, with the gold content increasing from 1.21% for MWCNT-Au_{nano} to 2.86% for *Ox*.MWCNT-Au_{nano}.

3.3 Electrochemical detection of Cr(VI)

The electrochemical detection of Cr(VI) was carried out in an acidified solution at a pH of 2.0 using H_2SO_4. This pH was selected as it is well known that the reduction of Cr(VI), which involves the transfer of protons, depends on the solution pH, with the peak potential shifting to higher potentials and the peak current increasing as the pH value is lowered [17]. The influence of pH is illustrated in Fig. 5 for the MWCNT-modified electrode. These data were obtained using cyclic voltammetry and by following the reduction peak associated with

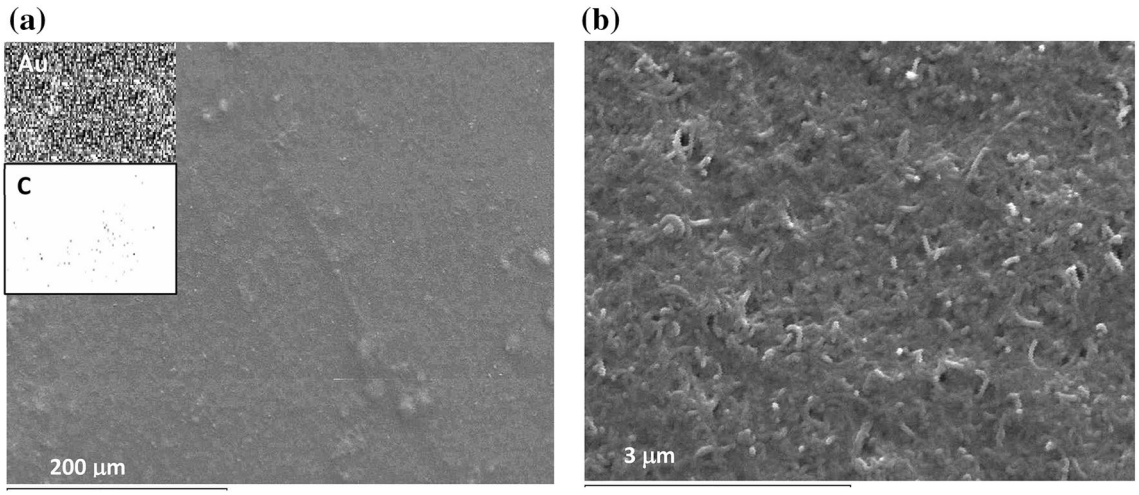

Fig. 4 **a** Low and **b** higher magnification SEM micrographs of the *Ox*.MWCNT-Au_{nano} composite modified Au electrode, formed from 20 µL of 10 mg mL^{-1} composite dispersion in DMF. Inset in **a** shows the mapping profiles for Au and C

Table 1 Percentage of C, O and Au obtained using EDX (n = 6) for the modified electrodes with Pt as the substrate

Material	C (wt%)	O (wt%)	Au (wt%)
MWCNT	98.82 ± 0.14	1.18 ± 0.14	–
MWCNT-Au_{nano}	98.02 ± 0.51	0.77 ± 0.51	1.21 ± 0.37
Ox.MWCNT-Au_{nano}	88.08 ± 0.39	9.06 ± 0.37	2.86 ± 0.16

the conversion of Cr(VI) to Cr(III) (at 0.57 V versus SCE, see Fig. 6a) the peak current and the corresponding peak potential were recorded as a function of the solution pH and are plotted in Fig. 5. It is clear that the peak current decreases as the pH increases and a higher signal is obtained in the more acidic solutions. It is also evident from the potential-pH plot that the reduction of Cr(VI) proceeds at more electropositive potentials in these acidic solutions. The reduction potential of Cr(VI) is well known to depend on the pH and the overall reaction is shown in Eq. (2). Using the Nernst equation, the relationship between the potential and pH can be written as, $E = A - 0.138\text{pH}$, where A includes E^0 and depends on the concentrations of Cr(VI) and Cr(III). This indicates a linear relationship with a slope of 138 mV. However, the level of agreement between this predicted pH-dependence and the observed pH is poor. A higher slope of 230 mV is evident for pH values between 2.0 and 3.5 and this is probably connected to the complexity of the Cr(VI) reduction reaction [17], where disproportion reactions and different oxidation states of Cr occur to give the overall conversion of Cr(VI) to Cr(III).

$$Cr_2O_7^{2-} + 14H^+ + 6e^- \rightarrow 2Cr^{3+} + 7H_2O \quad (2)$$

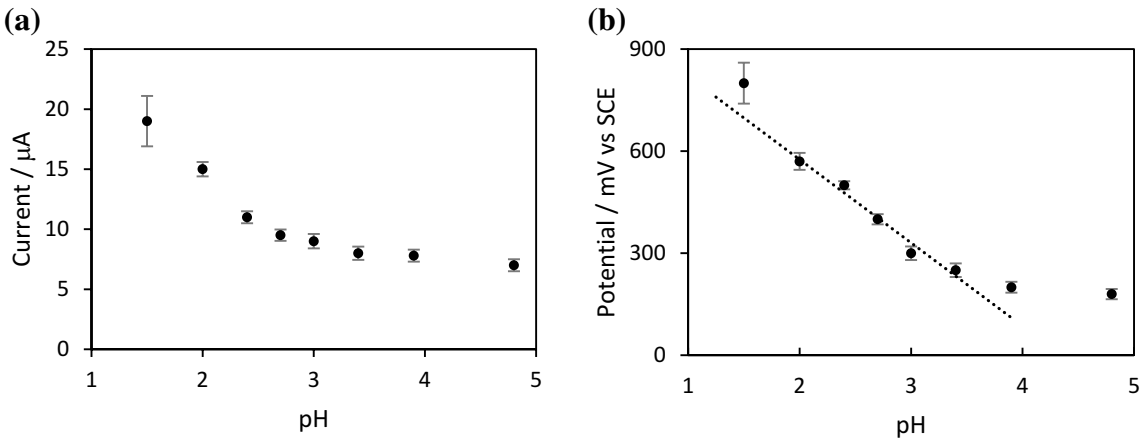

Fig. 5 **a** Peak current and **b** peak potential recorded using cyclic voltammetry at 10 mV s^{-1} in 0.4 mM Cr(VI) for MWCNT-Au_{nano} modified electrode ($n = 3$)

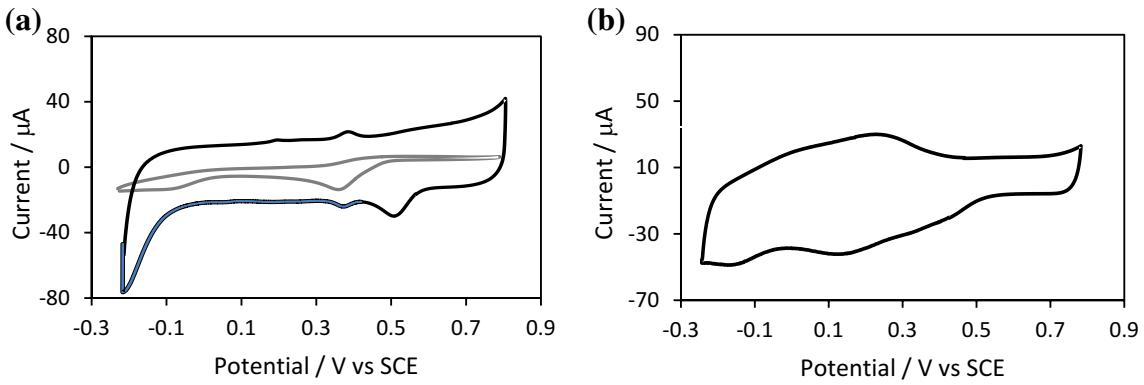

Fig. 6 Cyclic voltammograms of **a** grey line—Au and black line—Au modified with MWCNTs **b** black line—Au modified with the *Ox*. MWCNT-Au_{nano} composite recorded in 5.0×10^{-4} M Cr(VI) in H_2SO_4, pH 2.0 at a scan rate of 10 mV s^{-1}

It is also evident that higher errors are seen at a pH of 1.5 and this may be related to the oxidation or degradation of the carbon nanotubes. Indeed, Gu et al. [32] have shown that Cr(VI) can oxidise carbon nanotubes in acidic solutions, at a pH of 1.0, but no measureable oxidation was evident at a pH of 2.0. This is consistent with the lower errors seen at a pH of 2.0, Fig. 5. Therefore, a pH of 2.0 was selected to minimise the oxidation of the carbon nanotubes and to facilitate the reduction of Cr(VI).

Using the Pourbaix diagram for chromium [17], it is seen that $HCrO_4^-$ and $Cr_2O_7^{2-}$ are the chromium species that exist between a pH of 0.75 and 6.45, with the $HCrO_4^-$ being the predominant ion for Cr(VI) concentrations below 0.01 g L^{-1}. As these are anionic species, there may be some electrostatic repulsion between Cr(VI) and the carboxylate groups generated on the carbon nanotubes during reflux in HNO_3. However, the concentration of these groups is only at 6%, which is sufficient to facilitate dispersion of the nanotubes in solution, but not high enough to have any significant electrostatic repulsion with the Cr(VI) anions.

The response of the sensors to Cr(VI) was initially studied using cyclic voltammetry. Typical voltammograms recorded for gold, gold modified with MWCNTs and gold modified with *Ox*.MWCNT-Au_{nano} are shown in Fig. 6. These voltammograms were recorded in 5.0×10^{-4} M Cr(VI) at a scan rate of 10 mV s^{-1}. A well-defined reduction peak for Cr(VI) appears at 0.41 V versus SCE, with a peak current of 1.03×10^{-5} A for the gold electrode. The Cr(VI) reduction peak appears at a higher potential of 0.57 V versus SCE at the MWCNT-modified electrode and a higher peak current of 1.63×10^{-5} A is achieved. Other redox peaks are visible at 0.40 V versus SCE and these resemble an adsorbed redox couple. Zheng et al. [33] have attributed these redox waves to oxygen-containing functional groups on the MWCNTs. On the other hand, there is no well-defined reduction peak for Cr(VI) at the *Ox*.MWCNT-Au_{nano}-modified electrode. Again, the broad redox pair at about 0.20–0.30 V versus SCE, which is now more pronounced, is probably related to oxygen functionalities [33]. It appears that this broad wave combined with the high capacitance masks the Cr(VI) peak. While the capacitive current is relatively low at the higher potentials, it increases considerably as the potential approaches 0.50 V versus SCE. The shoulder peak at about 0.52 V versus SCE was attributed to Cr(VI) reduction, giving approximate peak potentials of 0.41 V for gold, 0.57 V for MWCNT-modified gold, and 0.52 V versus SCE for *Ox*. MWCNT-Au_{nano}-modified gold. This shows that the peak potential for the Cr(VI) reduction reaction is shifted to significantly higher potentials on modification of the gold electrode. The peak potentials are shifted to values between 0.52 V and 0.57 V versus SCE depending on the combination used, indicating that the Cr(VI) reduction, while taking place at both the carbon nanotubes and the gold particles, is particularly influenced by the carbon nanotubes. While the Cr(VI) reduction reaction can be followed using cyclic voltammetry at the MWCNT- and MWCNT-Au_{nano}-modified electrodes, the capacitance of the functionalised carbon nanotubes, *Ox*.MWCNT-Au_{nano}, is too high to enable the detection of Cr(VI) using voltammetry, and these voltammograms were only useful in establishing an appropriate potential for the detection of Cr(VI) using amperometry.

By using constant potential amperometry coupled with a rotating disc electrode, that facilitates mass transport, the capacitive current and any current arising from the electrochemistry of the oxygen-containing groups on the carbon nanotubes can be minimised by allowing the current to reach a steady state before the addition of Cr(VI) aliquots. Representative data recorded at a fixed potential of 0.40 V versus SCE for the *Ox*.MWCNT-Au_{nano} modified gold electrode are shown in Fig. 7. Similar data were recorded for the MWCNT- and MWCNT-Au_{nano}-modified electrodes, and unmodified gold (at 0.20 V vs. SCE) using a rotation speed of 1900 rpm. Once a steady-state current was obtained, successive aliquots of a Cr(VI) solution were

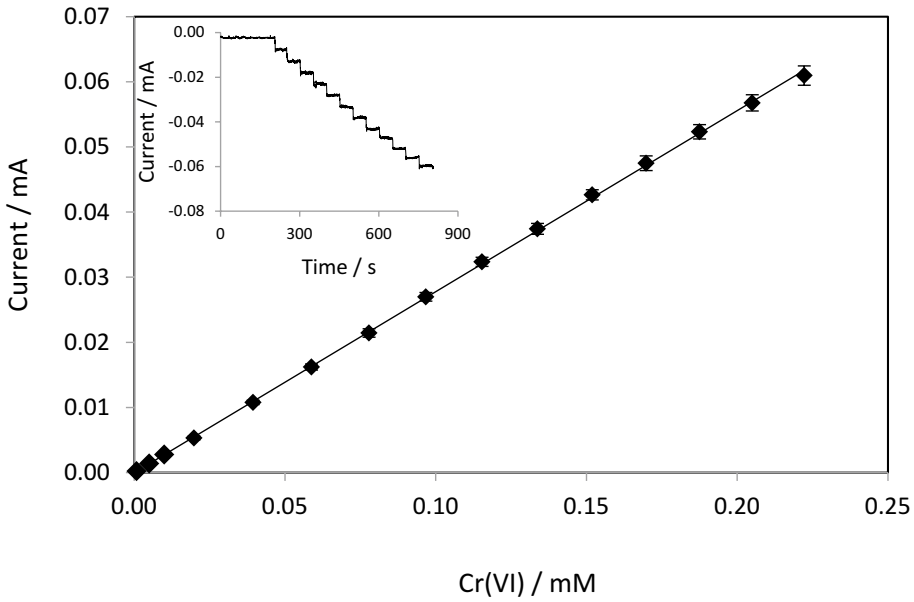

Fig. 7 Calibration curve for the reduction of Cr(VI) at the *Ox*.MWCNT-Au_{nano} composite-modified Au electrode, ($n=3$ and $R^2=0.99$) and amperometric response at 0.40 V versus SCE with a rotation speed of 1900 rpm (inset)

Table 2 LOD values for the Cr(VI) sensors using cyclic voltammetry and constant potential amperometry coupled with rotating disc voltammetry (CPA/RDE)

Sensor	LOD/M	
	Cyclic voltammetry	CPA/RDE
Au	7.40×10^{-5}	2.0×10^{-5}
Au/MWCNT	1.45×10^{-4}	1.9×10^{-6}
Au/MWCNT-Au_{nano}	1.55×10^{-4}	1.1×10^{-6}
Au/*Ox*.MWCNT-Au_{nano}	–	7.2×10^{-7}

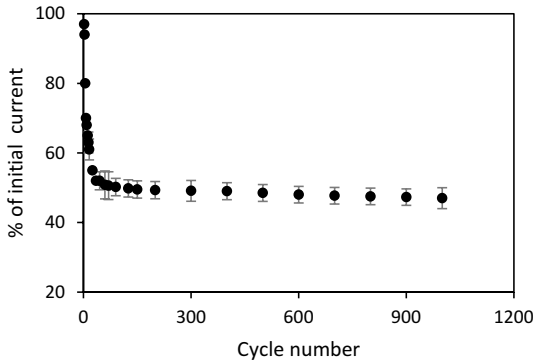

Fig. 8 Current with the % of the initial current recorded in cycle 1, plotted as a function of the cycle number recorded using cyclic voltammograms at 10 mV s^{-1} in a solution containing 0.6 mM Cr(VI) in H_2SO_4, pH 2.0 for MWCNT-Au_{nano} ($n=3$)

added to the continuously stirred solution in order to obtain the current–time response. This amperometric current–time response is shown in Fig. 7 (in the inset) with the accompanying calibration curve. The calibration curve shows very good linearity and reproducibility, with a sensitivity of 0.28 mA mM^{-1}. A limit of detection of 7.2×10^{-7} M (37 µg L^{-1}) was calculated, using Eq. (3), which satisfies the limits set by WHO of 9.61×10^{-7} M (50 µg L^{-1}). In Eq. (3), σ is the standard deviation of the baseline before the Cr(VI) was added. Furthermore, a current of 2.16×10^{-4} mA, that is easily measured experimentally, was obtained for a Cr(VI) concentration of 8.0×10^{-7} M.

$$\text{LOD} = 3(\sigma)/\text{Sensitivity} \quad (3)$$

The LOD values of the different modified electrodes are summarised in Table 2. While it is apparent from these data that the LOD of all the modified electrodes is nearly sufficient to meet the WHO limit, the *Ox*.MWCNT-Au_{nano}-modified electrode provides the best detection and lowest LOD. This shows that the presence of gold, which is well dispersed along the walls of the carbon nanotubes, with a reasonably uniform size, facilitates the rate of electron transfer. However, it is clear that the reduction of Cr(VI) occurs at the carbon nanotubes, as illustrated in Fig. 6a. It appears that the gold nanoparticles and carbon nanotubes provide a synergistic effect. This may be related to an increase in the surface area on decorating the carbon nanotubes with the gold nanoparticles, or to a more efficient electron-transfer reaction at the composite.

The stability of the MWCNT-Au_{nano} sensor was studied and is summarised in Fig. 8, where the peak current obtained using cyclic voltammetry at a scan rate of 10 mV s^{-1} and cycled between −0.20 and 0.70 V versus SCE is shown as a function of the cycle number. As detailed earlier, these non-functionalised carbon nanotubes have a lower capacitance and the Cr(VI) reduction wave can be followed. There is a significant decay in the peak current over the first 15 cycles;

however, steady-state conditions are achieved after about 20–25 cycles and then the current remains essentially constant. Although the peak current at this point has dropped by approximately 50%, the peak currents are reproducible and remain constant with continued cycling. There is no evidence for the degradation of the carbon nanotubes at these higher cycles where steady-state conditions are maintained.

The selectivity of the sensors to Cr(VI) reduction in the presence of potential interferences was studied using cyclic voltammetry for the MWNCT- and MWCNT-Au_{nano}-modified electrodes, while constant potential amperometry coupled with rotating disc voltammetry was employed for the *Ox*.MWCNT-Au_{nano}-modified electrode. The concentrations of the interferences were selected based on the limits set for these species in water samples [34], which are 2.0 mg L^{-1} (3.2×10^{-5} M) for Cu(II), 50 mg L^{-1} (8.0×10^{-4} M) for nitrate and 250 mg L^{-1} (7.0×10^{-3} M) for chloride. There was no change in the peak potential on cycling the MWNCT or the MWCNT-Au_{nano}-modified electrodes in the presence of the interferences, indicating no significant interference. The influence of the interferences on the steady-state peak current at different concentrations is summarised in Fig. 9, where it is clear that both chloride and Cu(II) have no significant effect on the Cr(VI) reduction peak current. However, some interference is seen with the higher nitrate concentrations. Similar results were obtained with the MWCNT-Au_{nano}-modified electrode. The influence of interferences on the steady-state current for the *Ox*.MWCNT-Au_{nano}-modified electrode is also shown in Fig. 9. Again, it can be seen from this plot that the interference from these additions is negligible. As the applied potential is relatively high at 0.40 V versus SCE, the Cu(II) cations cannot be electrochemically reduced. There is no appreciable interference from the chloride anions and only a slight increase in the current with the nitrate anions even though chloride anions and particularly nitrate anions are well known to adsorb. Following the addition of these interferences, Cr(VI) was added and as shown in Fig. 9, the current increased in response to the injection of Cr(VI).

The selectivity of the sensor was studied further by using a real water sample. The analytical data provided with the water sample were as follows: 8.4 mg L^{-1} chloride; 0.03 mg L^{-1} orthophosphate; < 0.002 mg L^{-1} nitrite; < 0.3 mg L^{-1} nitrate; 0.03 mg L^{-1} ammonia; 0.05 mg L^{-1} total phosphorous and < 1 mg L^{-1} solids. The samples were filtered to remove solid particulates and then acidified to a pH of 2.0 using concentrated H_2SO_4. The solutions were then spiked with different concentrations of Cr(VI) and a calibration curve was obtained and compared to the data recorded using the acidified deionised water. These plots are presented in Fig. 10 where the MWCNT-Au_{nano}-modified electrode was used as the sensor and cyclic voltammetry was employed as the technique. The slope of the linear plot obtained in H_2SO_4 dissolved in deionised water was

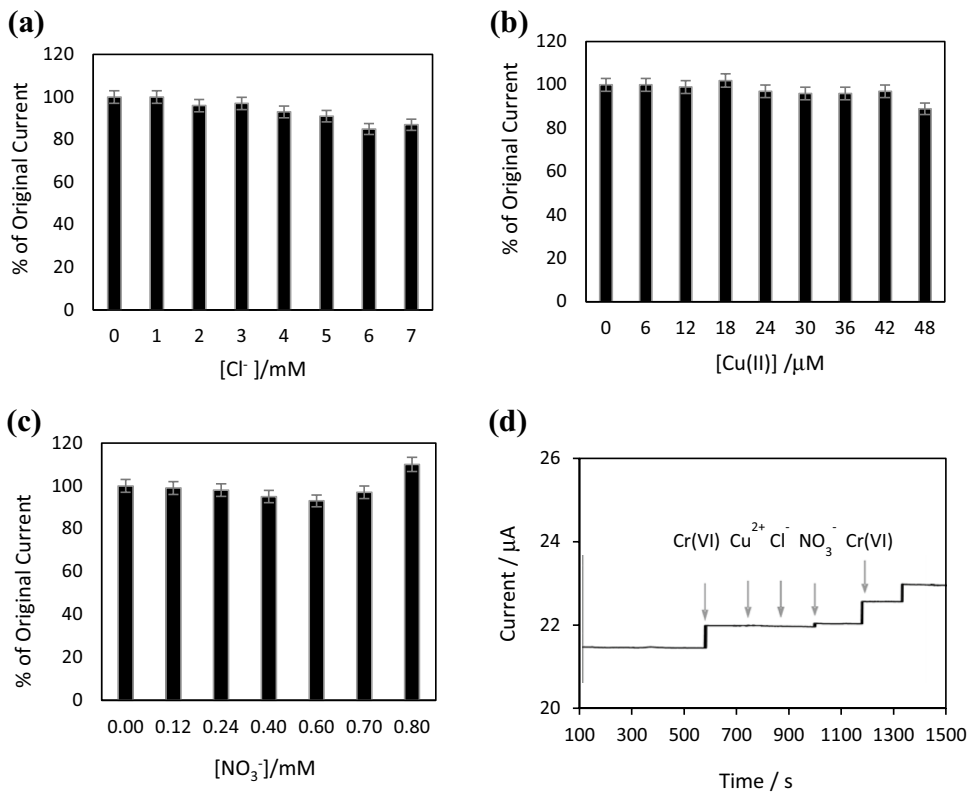

Fig. 9 Peak current expressed as a percentage of the current in the absence of any interferences shown as a function of the interference concentration for **a** Cl^-, **b** Cu^{2+} and **c** NO_3^- at the MWCNT-modified electrode ($n=3$) and **d** steady-state current measured in a 0.077 mM Cr(VI) solution in response to the addition of 32 µM Cu^{2+}, 7.0 mM Cl^- and 0.8 mM NO_3^- for the *Ox*.MWCNT-Au_{nano} composite

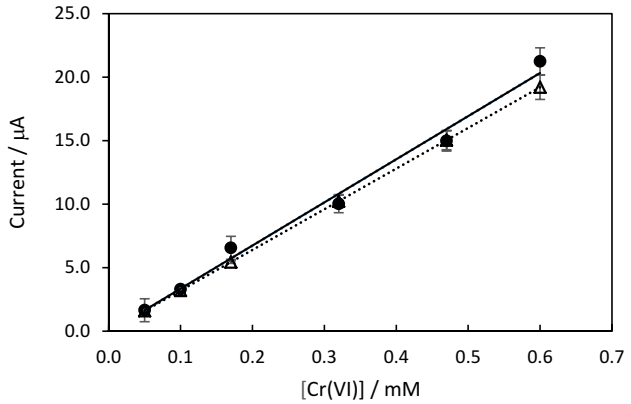

Fig. 10 Calibration curves recorded for MWCNT-Au_{nano} in dotted triangle—deionised water with H_2SO_4 ($R^2=0.99$) and in continuous line with circle—real water sample, acidified with H_2SO_4 ($R^2=0.98$), ($n=3$)

32 µA mM^{-1}, while the slope of the corresponding plot generated in the real water sample was slightly higher at 33 µA mM^{-1}. The errors were somewhat higher in the real water samples and this may be connected to solids that were not completely removed using the simple filtration step. Although the real water sample contains several species, including phosphates, nitrates, nitrites, ammonia and chlorides, the sensor is capable of detecting the Cr(VI) with little interference.

It is clear from Figs. 9 and 10 that the MWCNT-, MWCNT-Au_{nano}- and *Ox*.MWCNT-Au_{nano}-modified electrodes provide good selectivity. This seems to be partially connected to the relatively high Cr(V) reduction potentials, in the vicinity of 0.50–0.57 V versus SCE, which indicate a low overpotential for the Cr(VI) reduction reaction. At these potentials, the reduction of Cu(II), nitrites and nitrates is not feasible and the potentials are too high for the adsorption of nitrates or nitrites. In addition, the acidic H_2SO_4 has a cleaning effect, chemically dissolving any metal contaminants at the surface. Indeed, gold electrodes are frequently cycled in H_2SO_4 to give a clean surface [35]. Finally, the size and density of the gold nanoparticles may play a role. Tsai and Chen [36] have shown that larger gold nanoparticles deposited on indium tin oxide (ITO) electrodes gave a negative shift of the peak potential, lower peak currents and poor stability when used as a sensor. This was attributed to particle agglomeration. As shown in Fig. 2, the gold nanoparticles have diameters of approximately 7.5 nm and they are reasonably well dispersed which will prevent particle agglomeration and the formation of larger particles.

The *Ox*.MWCNT-Au_{nano}-modified electrode, with a LOD of 7.2×10^{-7} M, a linear range extending from approximately 8.0×10^{-7}–2.3×10^{-4} M and good selectivity in the presence of a number of interference species, compares well with the Cr(VI) sensors previously reported. For example, Welch et al. [17] obtained good selectivity for a polycrystalline gold electrode in the presence of Cu^{2+}, Ni^{2+}, Fe^{3+} and Cr^{3+} with a detection limit of 4.3×10^{-6} M. This selectivity is maintained with the *Ox*.MWCNT-Au_{nano} composite but a lower LOD value is achieved. While more impressive LOD values in the range of 1.0×10^{-8}–1.0×10^{-11} M have been reached for carbon- or gold-modified electrodes, as reported in the review by Jin and Yan [37], these sensors have a lower linear concentration range. The *Ox*.MWCNT-Au_{nano}-modified electrode gives a sufficient LOD value and an extended linear region. However, this Cr(VI) sensor, like other electrochemical sensors, is more efficient in an acidic environment. Therefore, in terms of real applicability, the analytes must be acidified before analysis and this adds an additional step in the preparation of the samples.

4 Conclusion

A composite material was formed by combining gold nanoparticles with MWCNTs using a relatively simple synthetic procedure. The gold nanoparticles were deposited onto the sidewalls of the nanotubes with the use of sodium borohydride, a strong reducing agent. No heat was required and the reaction was complete in 5 min. A narrow size distribution was apparent for the nanoparticles formed which mainly existed at 7.5 nm in diameter. The gold composition was estimated at 2.0–2.6 wt%. of the total composite. The composite was cast onto a gold electrode to form a uniform, adherent and homogeneous film. Using a combination of cyclic voltammetry and constant potential amperometry coupled with rotating disc voltammetry, the performance of the carbon nanotubes without any gold nanoparticles, gold-decorated carbon nanotubes, and gold-decorated functionalised carbon nanotubes in the detection of Cr(VI) was studied. The functionalised carbon nanotubes with well dispersed gold nanoparticles showed very good Cr(VI) detection, giving good selectivity and a limit of detection of 7.2×10^{-7} M, reaching the mandatory level of 50 µg L^{-1} set by the World Health Organisation.

Acknowledgements The authors would like to acknowledge funding from the Environmental Protection Agency, Ireland.

References

1. Zhitkovich A (2011) Chromium in drinking water: sources, metabolism, and cancer risks. Chem Res Toxicol 24:1617–1629
2. Anandasadagopan SK, Sundaramoorth C, Pandurangan AK, Nagarajan V, Srinivasan K, Ganapasam S (2017) S-Allyl cysteine alleviates inflammation by modulating the expression of NF-κB during chromium(VI)-induced hepatotoxicity in rats. Hum Exp Toxicol 36(11):1186–1200

3. Jin W, Zhang Z, Wu G, Tolba R, Chen A (2014) Integrated lignin-mediated adsorption-release process and electrochemical reduction for the removal of trace Cr(VI). RSC Adv 4:27843–27849
4. WHO (1993) Guidance for drinking water quality, second edition, vol 1, recommendations, WHO, Geneva, pp 45–46
5. Mohan D, Pittman CU (2006) Activated carbons and low cost adsorbents for remediation of tri- and hexavalent chromium from water. J Hazard Mater 137(2):762–811
6. McCarroll N, Keshava N, Chen J, Akerman G, Kligerman A, Rinde E (2010) An evaluation of the mode of action framework for mutagenic carcinogens case study II: chromium(VI). Environ Mol Mutagen 51(2):89–111
7. Lindsay DR, Farley KJ, Carbonaro RF (2012) Oxidation of CrIII to CrVI during chlorination of drinking water. J Environ Monit 14(7):1789–1797
8. Nan J, Yan X-P (2005) On-line dynamic two-dimensional admicelles solvent extraction coupled to electrothermal atomic absorption spectrometry for determination of chromium(VI) in drinking water. Anal Chim Acta 536(1–2):207–212
9. Inui T, Fujita K, Kitano M, Nakamura T (2010) Determination of Cr(III) and Cr(VI) at sub-ppb levels in water with solid-phase extraction/metal furnace atomic absorption spectrometry. Anal Sci 26(10):1093–1098
10. Elci L, Kartal AA, Soylak M (2008) Solid phase extraction method for the determination of iron, lead and chromium by atomic absorption spectrometry using Amberlite XAD-2000 column in various water samples. J Hazard Mater 153(1–2):454–461
11. Li Y, Pradhan NK, Foley R, Low GKC (2002) Selective determination of airborne hexavalent chromium using inductively coupled plasma mass spectrometry. Talanta 57(6):1143–1153
12. Shenashen MA, Shahat A, El-Safty SA (2013) Ultra-trace recognition and removal of chromium(VI) ions from water using visual mesocaptor. J Hazard Mater 244–245:726–735
13. Toal SJ, Jones KA, Magde D, Trogler WC (2005) Luminescent silole nanoparticles as chemoselective sensors for Cr(VI). J Am Chem Soc 127:11661–11665
14. Bergamini MF, dos Santos DP, Zanoni MVB (2007) Development of a voltammetric sensor for chromium(VI) determination in wastewater sample. Sens Actuators B 123(2):902–908
15. Vacek J, Mozga T, Cahová K, Pivoňková H, Fojta M (2007) Electrochemical sensing of chromium-induced DNA damage: DNA strand breakage by intermediates of chromium(VI) electrochemical reduction. Electroanalysis 19(19–20):2093–2102
16. Lin L, Lawrence NS, Thongngamdee S, Wang J, Lin Y (2005) Catalytic adsorptive stripping determination of trace chromium(VI) at the bismuth film electrode. Talanta 65(1):144–148
17. Welch CM, Nekrassova O, Compton RG (2005) Reduction of hexavalent chromium at solid electrodes in acidic media: reaction mechanism and analytical applications. Talanta 65(1):74–80
18. Tukur SA, Yusof NA, Hajian R (2015) Linear sweep anodic stripping voltammetry: determination of chromium(VI) using synthesized gold nanoparticles modified screen-printed electrode. J Chem Sci 127(6):1075–1081
19. Jin W, Wu G, Chen A (2014) Sensitive and selective electrochemical detection of chromium(VI) based on gold nanoparticle-decorated titania nanotube arrays. Analyst 139(1):235–241
20. Jena BK, Raj CR (2008) Highly sensitive and selective electrochemical detection of sub-ppb level chromium(VI) using nanosized gold particle. Talanta 76(1):161–165
21. Rosolina SM, Bragg SA, Ouyang R, Chambers JQ, Xue ZL (2016) Highly sensitive detection of hexavalent chromium utilizing a sol-gel/carbon nanotube modified electrode. J Electroanal Chem 781:120–125
22. Rudnitskaya A, Evtuguin DV, Costa LC, Graca MPF, Fernandes AJS, Correia MRP, Gomes MTSR, Oliveira JAPB (2013) Potentiometric chemical sensors from lignin-poly(propylene oxide) copolymers doped by carbon nanotubes. Analyst 138(2):501–508
23. Hasnahena S, Roy M (2018) Sensing of low concentration of ammonia at room temperature by decorated multi-walled carbon nanotube: fabrication and characteristics. Appl Phys A 124(1):1–9
24. Beiranvand S, Azadbakht A (2017) Electrochemical switching with a DNA aptamer-based electrochemical sensor. Mater Sci Eng C 76:925–933
25. Moreno-Guzmán M, Agüeí L, González-Cortés A, Yáñez-Sedeño P, Pingarrón JM (2013) Gold nanoparticles/carbon nanotubes/ionic liquid microsized paste electrode for the determination of cortisol and androsterone hormones. J Solid State Electrochem 17(6):1591–1599
26. Afkhami A, Soltani-Felehgari F, Madrakian T, Ghaedi H (2014) Surface decoration of multi-walled carbon nanotubes modified carbon paste electrode with gold nanoparticles for electro-oxidation and sensitive determination of nitrite. Biosens Bioelectron 51:379–385
27. Wang Z, Shirley MD, Meikle ST, Whitby RDL, Mikhalovsky SV (2009) The surface acidity of acid oxidised multi-walled carbon nanotubes and the influence of in-situ generated fulvic acids on their stability in aqueous dispersions. Carbon 47(1):73–79
28. Hanelt S, Orts-Gil G, Friedrich JF, Meyer-Plath A (2011) Differentiation and quantification of surface acidities on MWCNTs by indirect potentiometric titration. Carbon 49(9):2978–2988
29. Sreeja R, Aneesh PM, Hasna K, Jayaraj KM (2011) Linear and nonlinear optical properties of multi walled carbon nanotubes with attached gold nanoparticles. J Electrochem Soc 158(10):K187–K191
30. Hou X, Wang L, Wang X, Li Z (2011) Coating multiwalled carbon nanotubes with gold nanoparticles derived from gold salt precursors. Diam Relat Mater 20(10):1329–1332
31. Cullity BD (1956) Elements of X-ray diffraction. Addison-Wesly, Boston
32. Gu H, Rapole S, Haung Y, Cao D, Luo Z, Wei S, Guo Z (2013) Synergistic interactions between multi-walled carbon nanotubes and toxic hexavalent chromium. J Mater Chem 1(6):2011–2021
33. Zheng H, Lin L, Okezaki Y, Kawakami R, Sakuraba H, Ohshima T, Takagi K, Suye SI (2010) Electrochemical behavior of dye-linked-proline dehydrogenase on glassy carbon electrodes modified by multi-walled carbon nanotubes. J Nanotechnol 1:135–141
34. Environmental Protection Agency (2010) The provision and quality of drinking water in Ireland. A report for the year 2010. Environmental Protection Agency, Washington, DC, pp 102
35. Colaianni L, Kung SC, Taggart DK, Picca RA, Greaves J, Penner RM, Cioffi N (2014) Reduction of spectral interferences using ultraclean gold nanowire arrays in the LDI-MS analysis of a model peptide. Anal Bioanal Chem 406(19):4571–4583
36. Tsai MC, Chen P-Y (2008) Voltammetric study and electrochemical detection of hexavalent chromium at gold nanoparticle-electrodeposited indium tinoxide (ITO) electrodes in acidic media. Talanta 76(3):533–539
37. Jin W, Yan K (2015) Recent advances in electrochemical detection of toxic Cr(VI). RSC Adv 5:37440–37450